Applied Computer Science, vol. 20, no. 4, pp. 39–62
doi: https://doi.org/10.35784/acs-2024-39

Submitted: 2024-08-29 | Revised: 2024-10-06 | Accepted: 2024-10-10

Keywords: diabetes mellitus, explainable ML, electrocardiogram, non-invasive method, photoplethysmography, feature extraction

Reehana SHAIK [0000-0002-2189-3616]*, *Ibrahim SIDDIQUE* [0000-0003-3310-6090]*

NOVEL MULTI-MODAL OBSTRUCTION MODULE FOR DIABETES MELLITUS CLASSIFICATION USING EXPLAINABLE MACHINE LEARNING

Abstract

Diabetes Mellitus (DM) is a persistent metabolic disorder which is characterized by increased blood glucose level in the blood stream. Initially, DM occurs while the insulin secretion in the pancreas has a disability to secrete or to use hormone for the metabolic process. Moreover, there are different types of DM depending on the physiological process, and the types include Type1 DM, Type2 DM and Gestational DM. Electrocardiography (ECG) waves are used to detect the abnormal heartbeats and cannot directly detect DM, but the wave abnormality can indicate the possibility and presence of DM. Whereas the Photoplethysmography (PPG) signals are a non-invasive method used to detect changes in blood volume that can monitor BG changes. Furthermore, the detection and classification of DM using PPG and ECG can involve analyzing the functional performance of these modalities. By extracting the features like R wave (W1) and QRS complex (W2) in the ECG signals and Pulse Width (S1) and Pulse Amplitude Variation (S2) can detect DM and can be classified into DM and Non-DM. The authors propose a Novel architecture in the basis of Encoder Decoder structure named as Obstructive Encoder Decoder module. This module extracts the specific features and the proposed novel Obstructive Erasing Module remove the remaining artifacts and then the extracted features are fed into the Multi-Uni-Net for the fusion of the two modalities and the fused image is classified using EXplainable Machine Learning (EX-ML). From this classification the performance metrics like Accuracy, Precision, Recall, F1-Score and AUC can be determined.

1. INTRODUCTION

Diabetes mellitus (DM) is a chronic metabolic disorder characterized by elevated blood glucose levels over an extended period of time. This condition is obvious when the pancreas fails to produce efficient insulin or when the body's cells exhibit minimal responsiveness to insulin or sometimes both factors simultaneously (Shashikant et al., 2021). As per the World Health Organization (WHO), about 555.6 million instances were recognized in 2022, with projections demonstrating a rise to 748.2 million by 2049. Diabetes is expanding swiftly in middle- and low-income nations, possibly attributable to its chronic nature and genetic

*VIT-AP University, India, skreehana.15@gmail.com, siddique.ibrahim@vitap.ac.in

predispositions, producing it the seventh commonest cause of death globally. Insulin, a hormone produced by the pancreas, promotes the entry of glucose into cells, where it serves as an energy source. In cases where insulin lacks efficiency or is inadequate, glucose assembles in the bloodstream instead of being used by cells (Kulkarni et al., 2023). This collection results in increased blood sugar levels, potentially yielding rise to a range of complications. Diabetes presents in diverse forms, including Type 1 Diabetes, wherein the immune system inaccurately targets and removes the insulin-producing beta cells within the pancreas. Hence, the body's capacity to produce insulin is notably diminished, if not entirely absent (Shaan et al., 2023). Type 1 diabetes usually develops in childhood in adults, although it can be seen at any stage of life. On the other hand, type 2 diabetes signifies the predominant form, including the bulk of diabetes cases. This condition develops when the body rises resistance to insulin or fails to produce minimal amounts of insulin needed to regulate blood sugar levels within the normal range (Dave et al., 2024). Type 2 diabetes is commonly linked to lifestyle elements like obesity, sedentary behaviour, and unhealthy dietary habits. While it generally emerges during adulthood, there is a growing trend of diagnosis among children and adolescents, validated to the increase in rates of obesity. Two crucial aspects concerning these estimations merit attention. Firstly, the common assessment of diabetes prevalence worldwide is likely to fall short of reflecting the actual burden of the condition. Secondly, diabetes often leads to pre-diabetes a state that offers greater possibility for preventive interventions and proves efficient in preventing the onset of diabetes. So, early identification of pre-diabetes and diabetes holds main significance in collective activities to reduce the global burden of diabetes. It's worth noting that the criteria for diagnosing diabetes and pre-diabetes predominantly hinge on assessing blood glucose levels and haemoglobin A1c (HbA1c) concentrations. However, these methods pose challenges as they are invasive and not easily implementable as screening tools, particularly in low-resource environments.

The composition of the Electrocardiogram (ECG) signal serves as a sign of cardiac well-being. Through ECG analysis, anomalies precisely associated with heart function, such as cardiac arrhythmia, can be detected (Prabha et al., 2021). Furthermore, it can offer valuable insights into conditions like diabetes, which might not initially appear to be connected to heart health. Diabetes can lead to complications affecting multiple organs, increasing the risk of premature mortality. While ECG has traditionally been employed in cardiac and medical domains, its commercial viability is now being investigated in diverse and innovative applications. In recent years, there has been a growing effort to create computer-based automated diagnostics for ECG readings (Mishra et al., 2024). Additionally, ECG has shown as a tool for detecting hyperglycemia and enabling continuous glucose monitoring in more recent developments.

Photoplethysmography (PPG) serves as a non-invasive method deploys optical technology to gauge volumetric changes in blood circulation. In this process, light released from an LED is directed onto the fingers or wrists, where it is either diffused or transmitted to a photodiode. The photodiode then calculates the detected light, presenting it in the form of a pulse wave (Hina & Saadeh, 2022). In transmissive mode PPG sensors, the photodiode is positioned on the opposite side of the LED, whereas in reflective mode, it is situated adjacent to the LED. PPG signals typically consist of both pulsed and non-pulsed components. One benefit is that the PPG signal can be obtained using devices already combines into daily life, such as smart phones and wristbands. In recent years, many studies have explored the potential of using PPG signals, coupled with traditional, machine learning

(ML) or Deep learning (DL) techniques, to detect diabetes. PPG offers the advantage of easily capturing sequential heartbeats, allowing for the measurement of both heart rate (HR) and heart rate variability (HRV) (Shaan et al., 2022). HRV signal, derived from the ECG, is generally calculated from the R–R interval. Likewise, in computing the HRV signal from the PPG signal, the inter-beat interval (IBI) or pulse interval (PPI) is employed. HRV estimates the variability in time durations between consecutive heartbeats, a method completely used as an indicator for variety health conditions (Lee et al., 2023). The HRV serves as a robust reflection of both the parasympathetic and sympathetic branches of the autonomic nervous system (ANS). The ANS controls the body's metabolic functions, crucially influencing the regulation of blood glucose levels.

Artificial intelligence (AI) indicates an intelligent system capable of following the expertise of medical professionals, aiding healthcare providers in their daily tasks and supports for decision-making and problem-solving processes. The combination of the ECG and PPG signal dataset with AI enables the prediction of blood glucose levels (BGL). The authors proposed a novel framework named as Obstructive Encoder Decoder Network for feature extraction. In this module the ReMEM encoder module extracts the specific features and provides it into the Obstructive Erasing Module where the remaining artifacts are fully refined and fed into the ReMDM decoder and finally the extracted features are fused using Multi-Uni-Net and DM is classified using Explainable ML.

1.1. Description of the proposed flow

The Obstructive Encoder-Decoder Module is designed to help in processing and analyzing signals from ECG and PPG data, the brief workflow description is provided below:

- Wave Extraction: After the initial preprocessing step, specific waves are extracted:
- ECG Data: Two main features are extracted: W1, which is the R-wave, and W2, representing the QRS Duration.
- PPG Data: Two features are also extracted: S1, which measures the Pulse Width, and S2, the Pulse Amplitude Variation.
- Noise Removal: Although most noise is removed in preprocessing, some motion and signal artifacts may still remain. For these, an Obstructive Erasing Module is used, which refines the signals to ensure higher accuracy in the next stages.
- Feature Extraction and Fusion: After the signals are cleaned, the Decoder extracts the refined features. These are then input into the Multi-Modality Unifying Network, where ECG and PPG features are combined.
- Classification: Finally, the fused features are used to classify the data with an Explainable ML Model, which not only identifies patterns but also provides insight into how it made these classifications.
- Metric Detection: This process allows to detect key metrics, which are crucial for understanding and diagnosing conditions such as DM.

1.2. Major contributions

- The novel contribution in this study is incorporating the Obstructive Erasing Module in the encoder decoder structure which helps to eliminate the artifacts in the ECG

and PPG signals that persists after preprocessing and the refined features are further processed to decoder.

- For classification of DM, EXplainable-ML is used which has an enhanced interpretability and it is crucial in understanding the decision-making process.

1.3. Motivation

- Enhanced Accuracy in Diabetes Detection: Existing methods of diabetes detection may lack precision, mainly when studying complex signals. By implementing a multi-level fusion approach (Focus Wave Blend, TwinPath Module, and MultiBlend fusion), this study aims to improve classification accuracy, specificity, and sensitivity, potentially leading to more reliable and early diagnosis of diabetes.
- Overcoming Limitations in Signal Fragmentation: Many existing methods only analyze isolated segments of ECG signals, which can lead to incomplete or inaccurate assessments. By fusing features from F1, F2, and F3 fragments, this research applies a more comprehensive signal analysis, allowing for a more holistic approach to diabetes detection.
- Innovative Use of Fusion Techniques for Signal Analysis: The combination of multiple fusion techniques in this study addresses the challenges of integrating distinct waveforms (such as the 'R', 'T', and 'QT' Waves) and maximizes their diagnostic value. This approach can contribute to the development of more advanced analytical frameworks in biomedical signal processing.

2. LITERATURE REVIEW

Ahamed et al. (2023) targets on using DL techniques for non-invasive detecting anomaly in ECG signals, with a particular attention on diabetes-related anomalies. It aims to improve the accuracy and reliability of anomaly detection using advanced DL models. Cordeiro et al. (2021) analyzes the use of DL methodologies to find hyperglycemia from ECG signals. By using the power of DL algorithms, the study aims to elevate accurate and efficient models for early detection of hyperglycemic episodes utilizing ECG data. Navaneethakrishna and Manuskandan (2021) looks into the analysis of HRV in ECG signals, differentiating patterns between normal and diabetic individuals. Utilizing a fragmentation approach, the study has a motive to uncover distinctive HRV patterns associated with diabetes, offering insights into potential diagnostic markers. Jain et al. (2023) suggested a features removal method for differentiate normal and diabetic ECG data. The single-lead ECG signal is charged to ten characteristics extraction processes; they are logging energy, threshold, Shannon, sure entropy, root mean square value, kurtosis, skewness, maximum value, energy, and variance. The Fisher-score has been adopted in feature ranking techniques. The ranked features are provided into classifiers. Li et al. (2021) proposed Three blood glucose ranges—low, moderate, and high can be non-invasively monitored thanks to an ECG-based technique that addressed the necessity of monitoring different blood glucose ranges for the management of diabetes. The abbreviation CNN-DBSCAN stands for spatial grouping of applications using density-based methods with convolution neural networks and noise. A method for classifying BG range-based ECGs and pre-processing ECG outliers was presented.

Srinivasan and Foroozan (2021) proposes a non-invasive method for diabetes prediction using PPG signals and DL techniques. By adopting the performance of DL, the study aims to develop a robust predictor that can accurately detect diabetes risk factors from PPG signals. Zanelli et al. (2023) proposes a method for detecting type 2 DM utilizing a Light CNN from a single raw PPG wave. The research aims to progress a reliable and efficient model capable of accurately diagnosing type 2 DM from PPG signals. Susana et al. (2023) investigates the non-invasive classification of BG levels by using PPG signals and time-frequency analysis techniques. By examining the spectral characteristics of PPG signals, the study aims to progress a robust classification model for approximating BG levels. Susana et al. (2022) motivates on emerging a non-invasive method for classifying BG levels to allow early detection of DM using PPG signals. By using ML techniques, the research aims to figure a reliable classifier proficient of accurately predicting BG levels from PPG data. Khan et al. (2023) proposes an expert diagnostic system for detecting hypertension and DM using discrete wavelet decomposition of PPG signals and ML techniques. By examining the incidence components of PPG signals, the purpose of the study to develop an accurate diagnostic tool for detecting hypertension and DM. Sathish et al. (2024) discussed a non-invasive technique for dividing cases into those with and without diabetes. One of the main drawbacks of commercially available invasive blood glucose level monitoring systems for patients is the discomfort, pain, and infection they may feel during the finger-prick blood sample collection process. Using a near-infrared sensor (NIR), a revolutionary non-invasive gadget is being considered for blood sugar classification. Singha and Ahmad (2021) proposed a straightforward technique that measured both HR and BGL values concurrently using a single instrument based just on PPG without pricking a finger or the need for a skilled individual. A pulse sensor is implemented to gather PPG signals. Moreover, the bandpass filter is used to extract noise from the PPG signal and increase it before sending it to the microcontroller unit (MCU). Gupta et al. (2022) suggested a unique indicator called the dynamic systemic vascular resistance index (dSVRI) to differentiate who are healthy and diabetes. It is based on systemic vascular resistance pathology. The time-domain PPG features that are currently in use and their higher derivatives were compared with the suggested dSVRI's diagnostic performance and discrimination capacity. Sen Gupta et al. (2021) proposed and creates a multifunctional, commercial prototype PPG device, which monitors the essential health indicator parameters. By improving the skin with red, green, and infrared LEDs the produced fingertip PPG gadget consists of both transmissive and reflecting type data gathering system. Particular emphasis is placed on indicating the accuracy of the blood glucose meter (BGL). Prabha et al. (2022) proposed unique Mel frequency spectral coefficients feature of the wristband PPG signal and physiological data are utilized to present the design of a non-invasive blood glucose determination system. A dataset of 217 participants from a hospital located in Cuenca, Ecuador is used to verify the proposed model. By using SVR, XGBR approaches Blood glucose levels (BGL) are predicted. Mishra and Nirala (2023) used a variety of machine learning (ML) approaches to offer a non-invasive method for classifying type 2 diabetes by utilizing brief PPG signals. For making it easier for people to diagnose type 2 diabetes early on ML classifier can be used to smart or wearable apps. More over 68 statistically relevant features were exposed to a variety of ML approaches, either with or without feature selection technique (FST). Li et al. (2024) aimed was to build a unique multimodal framework based on the merging of ECG and PPG signals to create a universal BG monitoring model. This is implemented as a

weight-based Choquet integral for BG monitoring spatiotemporal decision fusion approach. Moreover, three feature selection methods are utilized to find the appropriate temporal statistical features, and DNN to compact the spatial morphological data.

Tab. 1. Brief Analysis on the research gaps

Ref. No	Objective	Method/Algorithm	Limitation
(Ahamed et al., 2023)	Detect diabetes-related anomalies in ECG signals using DL.	DL	Model accuracy may vary with signal quality and noise.
(Cordeiro et al., 2021)	Identify hyperglycemia by analyzing ECG signals with DL.	Deep neural networks for ECG data classification.	Lack of generalizability across diverse populations.
(Navaneethakrishna & Manuskandan, 2021)	Differentiate HRV between normal and diabetic ECG signals.	Fragmentation of ECG signals and variability analysis.	Limited to specific ECG fragments, potentially overlooking broader patterns.
(Jain et al., 2023)	Automatically detect diabetes from ECG signals non-invasively.	ML	High dependency on signal preprocessing for accurate results.
(Li et al., 2021)	Monitor glucose levels using ECG to categorize into three ranges.	DBSCAN clustering and CNN for ECG-based classification.	Accuracy might be influenced by patient variability and signal noise.
(Srinivasan & Foroozan, 2021)	Predict diabetes non-invasively using PPG signals.	DL	May face challenges in handling noisy PPG data.
(Zanelli et al., 2023)	Detect Type 2 diabetes from a single PPG waveform.	Lightweight CNN for PPG signal processing.	Single-wave analysis may limit the robustness of results.
(Susana et al., 2023)	Classify blood glucose levels non-invasively using PPG.	Time-frequency analysis on PPG signals.	Time–frequency resolution may affect classification accuracy.
(Susana et al., 2022)	Detect diabetes early by classifying glucose levels with PPG.	ML	Model may be sensitive to PPG signal artifacts.
(Khan et al., 2023)	Detect hypertension and diabetes using wavelet decomposition of PPG	Discrete wavelet transform and ML algorithms	High computational complexity due to wavelet decomposition
(Sathish et al., 2024)	Develop a non-invasive system to detect diabetes from PPG.	ML	Limited performance in the presence of noisy signals
(Singha & Ahmad, 2021)	Estimate heart rate and glucose levels non-invasively with PPG.	Signal processing techniques on PPG data.	Low accuracy for glucose estimation across all ranges.
(Gupta et al., 2022)	Diagnose Type-II diabetes early with a novel PPG feature.	DL	Feature robustness requires further validation
(Sen Gupta et al., 2021)	Measure blood glucose non-invasively using an all-purpose PPG system.	ML	Performance varies across different demographic groups
(Prabha et al., 2022)	Estimate glucose levels using wrist-worn PPG and other parameters	PPG signal processing combined with physiological data.	Device-dependent, affected by motion artifacts
(Mishra & Nirala, 2023)	Classify Type 2 diabetes from short PPG signals.	ML.	Short signals may limit feature richness and accuracy.
(Li et al., 2024)	Monitor glucose non-invasively by fusing ECG and PPG features.	Spatiotemporal feature fusion and Choquet Integral model.	Complex model structure may lead to high computational demand.
(Pal & Mahadevappa, 2023)	Detect cardiac morbidities using fused ECG and PPG signals.	Dual attentive DCNN on fused ECG and PPG signals.	High data processing requirements due to dual modality

Pal and Mahadevappa (2023) suggested a novel approach for successfully identifying and categorizing heart abnormalities other than coronary artery disease and disorders connected to electrical impulses. 300 patients with cardiovascular illness had their PPG and ECG signals jointly possessed by following predetermined inclusion and exclusion criteria. The PPG and ECG signals are merged with an algorithm to create a fused signal. Skip connections, multidimensional convolution, and self and cross attention features are utilized in DNN construction.

3. PROPOSED METHODOLOGY

3.1. Data preprocessing

The presented Novel Framework follows an encoder -decoder structure, fusing the features extracted and classifying DM through distinct models. Overcoming the complexities inherent in extracting relevant features from ECG and PPG signals for diabetes classification is a significant challenge. However, using advanced techniques such as obstructive encoder-decoder networks, it can prominently provide a solution. These methodologies enable the model to effectively learn representations directly from the input data, thereby capturing the intricate patterns essential for accurately classify DM. Encoder - Decoder architectures can easily accommodate multimodal data and have capacity to incorporate multiple input channels into the model. Finally, we utilize Explainable ML to evaluate the classification results.

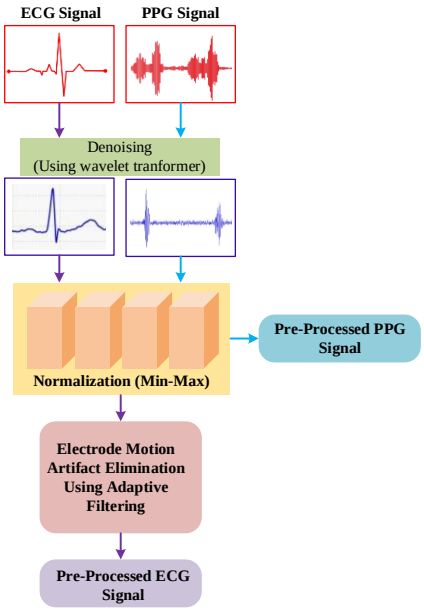

Fig. 1. The process flow of pre-processing

3.1.1. Pre-processing

In ECG signal pre-processing methods include denoising using Wavelet Transformer, Electrode motion artifact Elimination utilizing High-pass filter and normalization using min-max scaling. These methods are described below and in Fig. 1.

- Denoising: Noises of various kinds can distort any digital transmission. It is required to remove noise from signal features in order to isolate them. A noise-distorted ECG signal can be expressed as follows:

$$\mathbb{E}(\mathbb{S}) = \mathbb{WN}(\mathbb{S}) + \mathbb{O}(\mathbb{S}) \tag{1}$$

Here $\mathbb{E}(\mathbb{S})$ is the signal in ECG, $\mathbb{WN}(\mathbb{S})$ ECG with decreased noise distortion,$\mathbb{O}(\mathbb{S})$ECG signal with Noise. Wavelet transformer is a common tool for eliminating noise from ECG signals. The noise in the ECG readings was eliminated using the Discrete Wavelet Transform (DWT), a member of the Symlet family, Daubechies wavelet with a compact carrier and little asymmetry. Empirical techniques are used to establish the detail factor for each scenario. Three phases of wavelet transform are used to extract the ECG signal's noise. Using the DWT on a noisy signal is the first step in obtaining noisy wavelet coefficients. The next step after that is to choose an appropriate threshold. Finally, a guided inverse wavelet transform yields a signal that has been cleaned.

The DWT ECG signal is provided as follows:

$$\mathcal{WAVET}(\mathcal{X},\mathcal{Y}) = \frac{1}{\sqrt{2}}\sum_{\mathcal{f}=0}^{\mathbb{O}} \mathbb{E}_{\mathcal{f}} \int_{\mathcal{f}}^{\mathcal{f}+1} \beta\left(\frac{\mathbb{S}-\mathcal{Y}}{\mathcal{X}}\right) \mathcal{h}\mathcal{f} \tag{2}$$

Here $\mathbb{O}$ number of sample ECG signals, $\mathbb{E}$ is the distorted noise in ECG signal, symlet is denoted as β, the variables $\mathcal{X}$ and $\mathcal{Y}$ will take the values of:

$$\mathcal{X} = 1 \ldots . \mathcal{N}, \mathcal{Y} = 1 \ldots . \mathcal{N} - 1. \tag{3}$$

Simultaneously, this method is also implemented in PPG signal denoising.

Normalization: For normalizing the ECG and PPG signals, this Min-Max Normalization technique is used to scale the numeric features to a specific range; By scaling the signals to a common range, the larger scale feature can be prevented from dominating the analysis or adversely affecting the performance of algorithms that rely on distance metrics or optimization techniques. Moreover, to determine the minimum and maximum values of the ECG and PPG signals the normalization factor is calculated by:

$$\mathcal{NF} = \frac{\mathcal{DMV}-\mathcal{DMv}}{\mathcal{OMV}-\mathcal{OMv}} \tag{4}$$

Where $\mathcal{DMV}$ denotes the desired maximum value, $\mathcal{DMv}$ indicated the Desired Minimum Value, Original maximum value is noted by $\mathcal{OMV}$ and $\mathcal{OMv}$ denotes the original minimum value.

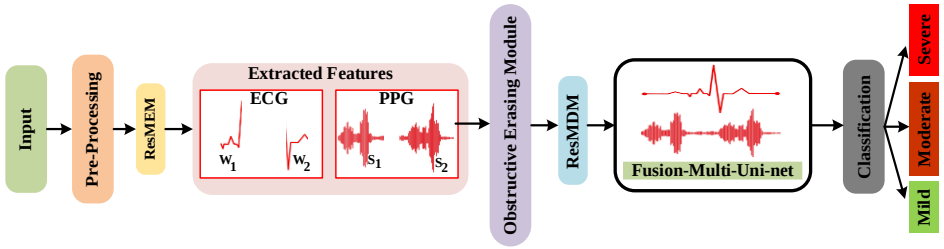

Fig. 2. The pipeline for the proposed framework

Electrode motion artifact Elimination: Electrode motion artifacts can occur due to factors such as the use of grouped electrodes or poor contact between dry electrodes and the skin. These issues can lead to instability in ECG recordings, making it challenging to assess the signal quality accurately. Addressing electrode motion artifacts is a major step in assessing the feature of ECG signals. We use the adaptive filtering method due to its ability to dynamically track signals in non-stationary conditions. Even in the absence of prior knowledge about the signal or noise characteristics, this method effectively filters out noise from the input by altering its impulse response. To appropriately filter each sample, the adaptive algorithm in adaptive filtering modifies the adaptable filter coefficients. Using the selected adaptive approach, filter coefficients are continuously modified.

$$\mathcal{P}(\mathfrak{n}) = \mathcal{ES}(\mathfrak{n}) + \mathcal{RE}(\mathfrak{n}) \tag{5}$$

$$\mathcal{RS}(\mathfrak{n}) \Rightarrow \mathcal{FS}(\mathfrak{n}) + \mathcal{RE}'(\mathfrak{n}) \tag{6}$$

$$\mathcal{ER}(\mathfrak{n}) = \mathcal{ES}'^{(\mathfrak{n})} = \mathcal{ES}(\mathfrak{n}) + \mathcal{RE}(\mathfrak{n}) - \mathcal{RE}'(\mathfrak{n}) \tag{7}$$

The mean squared value error signal minimizing is noted as $\mathcal{ER}(\mathfrak{n})$. The signal reference is noted to be $\mathcal{RS}(\mathfrak{n})$ and the input is processed through a digital filter to generate an output $\mathcal{RE}'(\mathfrak{n})$, The output aims to closely follows the replica of the noise and it is indicated as $\mathcal{RE}(\mathfrak{n})$.Following that, this signal output $\mathcal{FS}(\mathfrak{n})$ is subtracted from the primary input $\mathcal{P}(\mathfrak{n})$ to attain the assessed required signal $\mathcal{ES}'^{(\mathfrak{n})}$.

3.1.2. Obstructive encoder decoder module

This component comprises three sections: The Residual Multilevel Encoder Module (ReMEM), responsible for feature extraction. Despite artifact removal during pre-processing, certain motion and signal artifacts may remain unresolved. Therefore, the Obstructive Erasing Module is employed to address these noises. Following refinement, the Residual multilevel decoder module (ReMDM) where the feature level fusion of each modality is done and then fed into the Multi-Modality Unifying network for diabetes mellitus classification. The brief pipeline is shown in Fig. 2.

3.1.3. Residual multilevel encoder module (ReMEM)

In Distinct, we utilize the ReMEM technique shown in fig 3 to dynamically acquire the spatial fusion weights for feature maps across different scales.

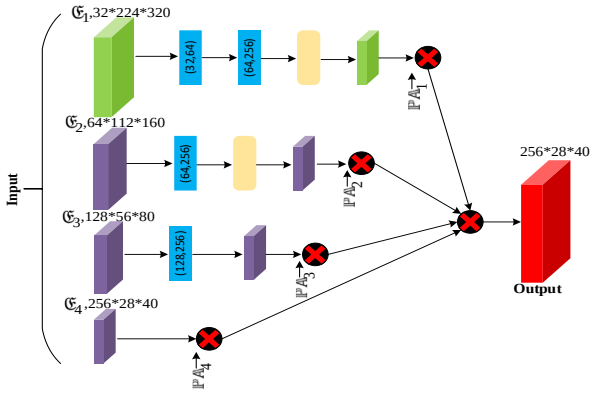

Fig. 3. Shows the structure of ReMEM

This approach simplifies the network in comprehensively capturing contextual features from the Specific data ECG waves named as W1(R-wave) and W2(QRS Duration) and significant PPG signals S1(Pulse Width) and S2 (Pulse Amplitude Variation) at the encoding stage. These significant W1 has been fragmented for a significant reason where the Individuals with a high resting heart rate and low HRV are at a heightened risk of developing DM in the future, whereas W2 wave was higher in DM individuals. In PPG signals S1 can be used in combination with additional physiological parameters, continuous BG monitoring systems offer enhanced monitoring capabilities and in S2 changes the parameter may denote the potential vascular abnormalities linked to diabetes, making its change in crucial for identifying the presence of DM.

However other methods that merge multi-level features through simple operations like element-wise sum or concatenation, the ReMEM approach introduced here dynamically learns the importance of features among various encoder levels. The ReMEM process involves two distinct steps: a) Equivalent rescaling and b) dynamic fusing. Initially, Convolution with a stride of 2 are employed to integrate features of varying scales into a unified 256 ×28 ×40, representation. Subsequently, Trainable weight parameter are applied to dynamically combine the features.

– Equivalent rescaling.

Features at level are denoted as the $\mathcal{L}\{\mathcal{L}\epsilon(1,2,3,4)\}$ and features in the encoder as $\mathbb{e}_{\mathcal{L}}$ related to $\mathfrak{E}_1, \mathfrak{E}_2, \mathfrak{E}_3$and $\mathfrak{E}_4$. As features across various levels exhibit in different resolutions and channels, they need to be standardized to the same size prior to fuse. We utilize $\mathbb{e}_{\mathbb{m}}^{\mathcal{L}}$ to indicate the rescaling operation feature $\mathbb{e}_{\mathbb{m}}$ to thefeature size of $\mathbb{e}_{\mathcal{L}}$. We need to merge $\mathfrak{E}_1, \mathfrak{E}_2, \mathfrak{E}_3$to the size $\mathfrak{E}_4$ (minimum to maximum), convolution with stride 2 and Soft-pool with stride 2 are utilized to feature rescaling. In this subgroup we represent $\mathcal{CN}_{\mathcal{T}}$ to denote the convolution with stride 2 and $\mathcal{S}_{\mathcal{P}}$ to denote the Soft-pool with stride 2. The distinct procedures for adjusting the dimensions of encoding features with varying sizes are outlined as follows:

$$\mathbb{e}_1^4 = \mathcal{S}_{\mathcal{P}}\left(\mathcal{CN}_{\mathcal{T}}\left(\mathcal{CN}_{\mathcal{T}}(\mathbb{e}_1)\right)\right) \tag{8}$$

$$\mathbb{e}_2^4 = \mathcal{S}_{\mathcal{P}}\left(\mathcal{CN}_{\mathcal{T}}(\mathbb{e}_2)\right) \tag{9}$$

$$\mathbb{e}_3^4 = \mathcal{S}_{\mathcal{P}}(\mathbb{e}_3) \tag{10}$$

$$\mathbb{e}_4^4 = \mathbb{e}_4 \tag{11}$$

– Dynamic fusing.

$\mathbb{e}_{\mathbb{m}}^{\mathcal{L}}$ Signifies the rescaling operation in the feature level $\mathbb{m}$ the feature in levelsize as $\mathcal{L}$. Theproposed output of the ReMEM is:

$$\mathcal{Y}_{\text{ReMEM}} = \mathbb{PA}_1 \times \mathbb{e}_1^{\mathcal{L}} + \mathbb{PA}_2 \times \mathbb{e}_2^{\mathcal{L}} + \mathbb{PA}_3 \times \mathbb{e}_3^{\mathcal{L}} + \mathbb{PA}_4 \times \mathbb{e}_4^{\mathcal{L}} \tag{12}$$

$\mathcal{L}$ is 4 and $\mathbb{PA}_1, \mathbb{PA}_2$, $\mathbb{PA}_3$ and $\mathbb{PA}_4$are parameters which are trainable, implying the features weight obtained by rescaling. Observe that $\mathbb{PA}_1, \mathbb{PA}_2$, $\mathbb{PA}_3$ and $\mathbb{PA}_4$these can be specific scalar variables that are shared across all channels uniformly. We force $\mathbb{PA}_1 + \mathbb{PA}_2 + \mathbb{PA}_3 + \mathbb{PA}_4 = 1$ and$\mathbb{PA}_1, \mathbb{PA}_2$, $\mathbb{PA}_3$,$\mathbb{PA}_4 \epsilon$ [0,1]. $\mathbb{PA}_n$ is elaborated as:

$$\mathbb{PA}_n = \frac{\varepsilon^{\gamma_n}}{\varepsilon^{\gamma_1} + \varepsilon^{\gamma_2} + \varepsilon^{\gamma_3} + \varepsilon^{\gamma_4}} \tag{13}$$

$n\epsilon\{1,2,3,4\} \times \mathbb{PA}_1, \mathbb{PA}_2$, $\mathbb{PA}_3$ and $\mathbb{PA}_4$are stated by utilizing the SoftMax function with $\gamma_1, \gamma_2, \gamma_3$ and γ_4 as the control parameters, each corresponding to a specific function and can be trained using standard backpropagation techniques.

3.1.4. Obstructive erasing module (OEM)

Even after the initial preprocessing stage removes artifacts, some remaining motion and signal irregularities may remain uncorrected. Figure 4 shows the overall architecture of the proposed framework. To efficiently handle these remaining noises, the authors propose the OEM for part feature erasing or recorrecting. The module comprises four sub-modules, each corresponding to a specific body part. Within each sub-module, there are two fully connected (FC) layers, one-layer normalization, and one Sigmoid function. Layer normalization is positioned between the FC layers, while the Sigmoid function resides at the final stage. The initial FC layer diminishes the channel dimension to a quarter of its original size, the objective of excluding particular details while regaining the original signal data that converts into a feature representation.

Following that, the final Sigmoid function initiates the predicted obstructive values$\mathcal{SG}_m$ for each part feature. We denote the operation as the multiplication of the obstructive scores with the corresponding part features as $\mathcal{OF}'$In terms of functionality, the process can be represented as follows:

$$\mathcal{OF}'_m = sigmoid\left(\mathfrak{W}_{\mathbb{rg}} \mathbb{NL}\left(\mathfrak{W}_{\mathbb{cp}} \mathcal{OF}_m\right)\right) \times \mathcal{OF}_m \tag{14}$$

Here $\mathfrak{W}_{\mathbb{cp}} \epsilon \mathrm{E}^{\mathrm{c}/4 \times \mathrm{c}}$, $\mathfrak{W}_{\mathbb{rg}} \epsilon \mathrm{E}^{\mathrm{c}/4 \times \mathrm{c}}$, $\mathbb{NL}$ is the normalization layer and m denotes m_{th} part feature. We compute the Mean Square Error (MSE) Loss between the obstructive masks and obstructive scores, which can be represented by the following function:

$$\mathrm{I}_{\text{mean}} = \frac{1}{N} \sum_{m=1}^{4} (\mathcal{SG}_m, \mathrm{MAS}_m) \tag{15}$$

3.1.5. Residual multilevel decoder module (ReMDM)

Multi-level fusion is typically used in computer vision, however improving scale fusion to enhance model presentation is still a difficult task. varying levels in encoder-decoder networks have varying receptive fields, which capture different types of data. In order to overcome this, ReMDM see fig 4 uses multiple pooling and multiple attention techniques to combine features from several levels.

We depict the characteristics at the level ,$\mathcal{L}$ in the decoder as $\mathrm{C}_{\mathcal{L}}\{\mathcal{L}\epsilon(1,2,3,4)\}$ corelated to ∂_1,∂_2,∂_3 and ∂_4 the resolution of C_1 is 224×320, which is the same as the input resolution of the network. $\mathrm{C}_{\mathcal{L}}^{1}$ represents the operation of rescaling feature $\mathrm{C}_{\mathcal{L}}$ to the size of feature C_1. This process is achieved through bilinear interpolation transformation, subsequently followed by 3 × 3 convolution. The former noted as $\mathbb{e}_{\vartheta}$ can be utilized to maximize the resolution of $\mathrm{C}_{\mathcal{L}}$to the resolution of C_1,the latter specifies as $\mathcal{CN}_{\mathcal{T}}$ can be given todecrease computational load, the channels of the resampled features are reduced to 4.

Fig:4 demonstrates the structure of ReMDM. The method for resizing the decoding features with distinct sizes includes merging the size of the four features to 4 × 224 × 320 after rescaling. We fuse them to form $\mathfrak{F}$.

$$\mathrm{C}_{\mathcal{L}}^{1}= \mathcal{CN}_{\mathcal{T}}\left(\mathbb{e}_{\vartheta}\left(\mathrm{C}_{\mathcal{L}}, 2^{\mathcal{L}-1}\right)\right), \quad \mathcal{L}\epsilon\{1,2,3,4\} \tag{16}$$

$$\mathfrak{F} = CONC\left(\mathrm{C}_{1}^{1}, \mathrm{C}_{2}^{1}, \mathrm{C}_{3}^{1}, \mathrm{C}_{4}^{1}\right) \tag{17}$$

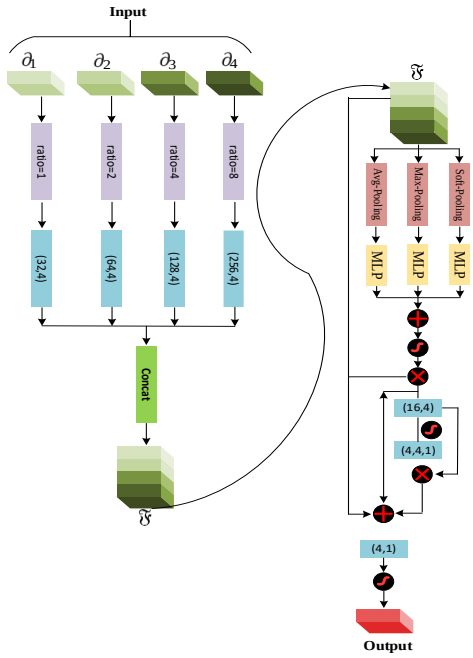

Fig. 4. Demonstrates the structure of ReMDM

We merge Avg-pool, Max-pool, and Soft-pool with multiple layer perception (MLP) to attain each channel co efficient of F. $\beta\epsilon[0,1]^{4\times1\times1}$ is noted as the scale coefficient attention

vector. In order to assign multi-level soft attention weight to each pixel, we insert a spatial attention block, which$\mathfrak{F} \times \beta$ as input to initiate spatial-wise attention coefficient $\delta\epsilon[0,1]^{1\times224\times320}$, so that $\beta \times \alpha$ denotes pixel-wise scale attention.The Spatial Attention contains one 3 × 3 and one 1 × 1 convolutional layer, The initial block provides 4 output channels followed by the Rectified Linear Unit (ReLU), while the following block gives 4 output channels followed by the Sigmoid function.First, the process combines convolution layers—each with the same number of output channels—with the bilinear interpolation technique. This combination functions to combine the features on different scales into a unified format, resulting in dimensions of 4 × 224 × 320.

The resulting output of the ReMDM model is:

$$C_{\mathrm{ReMDM}} = \mathfrak{F} \times \beta \times \alpha + \mathfrak{F} \times \beta + \mathfrak{F} \tag{18}$$

Residual connections are once more implied to aid in the training process. Through ReMDM, the network attains the capability to observe the most appropriate scale for the task.

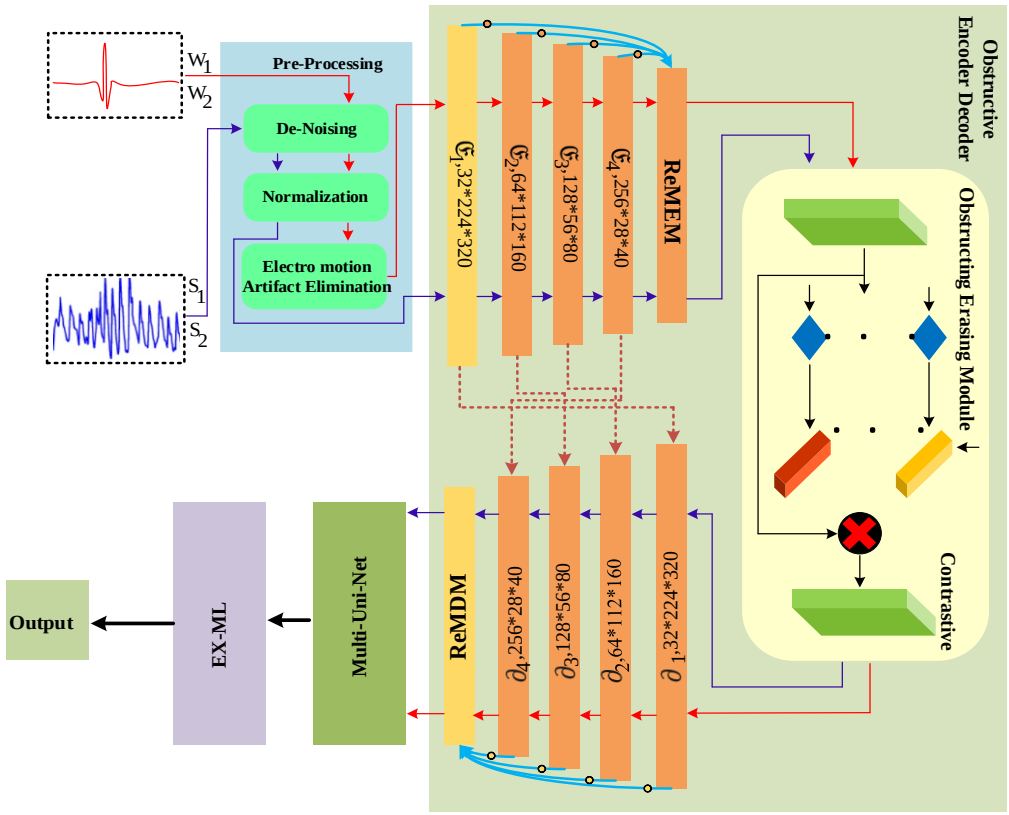

Fig. 5.The overall architecture of the proposed framework of obstructive encoder decoder module

3.1.6. Multi-modality unifying network (Multi-Uni-Net)

In order to consider the fundamental relationships between W1 and W2 waves and S1 and S2 data, the authors integrated a Multi-Uni-Net into their methodology. Particularly,

features were extracted independently from the ReMDM and subsequently input into the fusion module to enable thorough feature fusion. Within the fusion module, the inputs comprised ECG feature $\mathcal{W}_{i,j}$ and PPG feature$S_{i,j}$. These two features were initially transformed into $\mathcal{W} \epsilon \rho^{\mathcal{b}\times d}$ and $S \epsilon \rho^{\mathcal{b}\times d}$ by using FC layers, we estimated them into two various feature spaces. Additionally, the degree of similarity was calculated as follows:

$$\sigma_{ji} = \frac{exp(\mathcal{K}_{ij})}{\sum_{i=1}^{\mathcal{K}} exp(\mathcal{K}_{ij})}, \text{ where } \mathcal{K}_{ij} = \mathcal{Q}1(\mathcal{W}_i)^t \mathcal{H}_2(S_i) \tag{19}$$

$$\eta_{ji} = \frac{exp(\mathfrak{z}_{ij})}{\sum_{i=1}^{\mathcal{K}} exp(\mathfrak{z}_{ij})}, \text{ where } \mathfrak{z}_{ij} = \mathcal{Q}2(S_j)^t \mathcal{H}_1(\mathcal{W}_j) \tag{20}$$

Where $\mathfrak{S} = \mathcal{w} \times \mathcal{k}$ and σ, ηdenote the degree of correlation within the ECG waves and PPG data, respectively. Following that, the computed σ_{ji} and η_{ji} is the attention scores are multiplied with the feature values to produce the conclusive cross-modal attention maps. Subsequently, these maps are merged with the ECG features.$\mathcal{W}_i$ .After merging process, they are passed to subsequent FC layers, ultimately producing a fused prediction for DM.

3.1.7. Classification using EXplainable ML

EXplainable kNN provides a transparent decision-making mechanism within the algorithm, it generates the development trust and confidence in the predictions. This transparency allows users to understand how the model comes at its decisions, thereby improving their belief in the reliability of the model's development. EXplainable kNN shows numerous merits, such as transparency and interpretability, representing it as a valuable asset across various practical sections. These features are particularly advantageous in contexts where transparency and ease of interpretation play major roles in decision-making processes. This is accomplished by precisely choosing features, distance metrics, interpretation methodologies, and accounting for both local and global model behaviours. In kNN, classification depends on the closest of the nearest neighbors within a given space. Based on this, the allocation of data classes depends on the density of neighboring points in close availability to the target point. The output provided by kNN is determined by the closest neighbors, with uniform weights assigned to each. The distance formula calculates the absolute value of the difference between the coordinates in one dimension, and this computation is extended to multiple dimensions. It is represented as follows:

$$\omega(\mathcal{W}_{i,j}, S_{i,j}) = |\mathcal{W}_{i,j} - S_{i,j}| \tag{21}$$

$$\omega(\mathcal{W}_{i,j}, S_{i,j}) = \sqrt{(\mathcal{W}_{i,j} - S_{i,j})^2} \tag{22}$$

The final classification by using the kNN, has shown as:

$$\omega(\mathcal{W}_{i,j}, S_{i,j}) = \sqrt{(\mathcal{W}_{i,j} - S_{i,j})^2 + (\mathcal{W}_{i,j} - S_{i,j})^2} \tag{23}$$

4. EXPERIMENTAL EVALUATION

4.1. Training and testing data

4.1.1. ECG data

Primarily, a dataset consisting of 22,055 ECG records was gathered from 23 participants. Of these, 2,265 ECG records were excluded by the classifier, with 1,365 from 18 healthy individuals and 946 from 8 individuals with prediabetes or diabetes. Testing and training were conducted using the remaining 19,865 ECG recordings. Specifically, half of each participant's ECG records were selected at random to train the BG range monitoring model, while the remaining ECG records were assigned for testing.

4.1.2. PPG data

In the study, a group of 924 patients was randomly selected from the extensive MIMIC dataset. Figure 6 demonstrates the PPG Waveforms. Among these, data from 580 patients were reserved for training purposes, while data from the remaining 344 patients were allotted for testing manually. Within this group, 341 patients were diagnosed with diabetes. Among those diagnosed with diabetes, 180 were male, and 181 were female. Additionally, out of the total 584 patients diagnosed with hypertension, 300 were also found to have diabetes.

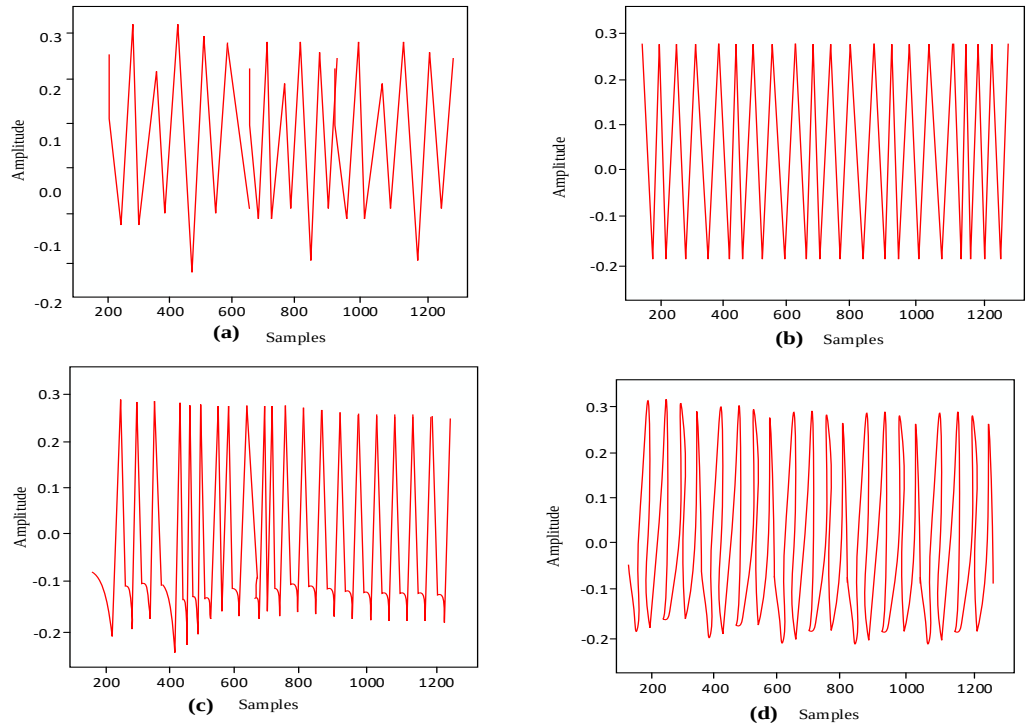

Fig. 6. Demonstrates the PPG Waveforms in 10 seconds a) and b) shows the diabetic patient PPG, c) and d) shows the non-diabetic patient PPG

4.2. Implementation details and performance evaluation

The experimental setup used for testing contains of a test bed equipped with a 2.40 GHz x64 Intel Core i9-6800 CPU, complemented by 32 GB of DDR8 RAM. Additionally, the system is augmented with a 6 GB NVIDIA GeForce RTX graphics card. Storage capacity is provided by a combination of 512 GB SSD and 2 TB HDD. The solid-state drive (SSD) comes pre-installed with Microsoft Windows 11 Professional 64-bit operating system. To optimize the training and testing procedures, the datasets and working settings are stored on the SSD. This approach eliminates the mechanical delays associated with the HDD, thereby facilitating the process. The true negative rate (TNR or specificity), true positive rate (TPR or sensitivity), positive predicted value (PPV), negative predicted value (NPV), and F-1 score are among the performance metrics we use to gauge how robust our system is. Below are the mathematical formulas for various performance metrics:

$$ACCURACY = \frac{\mathbb{T}^{\mathbb{P}}+\mathbb{T}^{\mathbb{N}}}{\mathbb{T}^{\mathbb{P}}+\mathbb{T}^{\mathbb{N}}+\mathbb{F}^{\mathbb{P}}+\mathbb{F}^{\mathbb{N}}} \times 100 \quad (24)$$

$$SPECIFICITY = \frac{\mathbb{T}^{\mathbb{N}}}{\mathbb{T}^{\mathbb{N}}+\mathbb{F}^{\mathbb{P}}} \times 100 \quad (25)$$

$$SENSITIVITY = \frac{\mathbb{T}^{\mathbb{P}}}{\mathbb{T}^{\mathbb{N}}+\mathbb{F}^{\mathbb{N}}} \times 100 \quad (26)$$

$$NPV = \frac{\mathbb{T}^{\mathbb{N}}}{\mathbb{T}^{\mathbb{N}}+\mathbb{F}^{\mathbb{N}}} \times 100 \quad (27)$$

$$F_1SCORE = \frac{2\times PRC\times TPR}{PRC+TPR} \quad (28)$$

$$PPV = \frac{\mathbb{T}^{\mathbb{P}}}{\mathbb{T}^{\mathbb{P}}+\mathbb{F}^{\mathbb{P}}} \times 100 \quad (29)$$

In this context, TP and TN denote the tally of accurately identified positive and negative occurrences, respectively. Correspondingly, FP and FN represent the counts of positive and negative events that were invalidly detected.

4.3. Results evaluation

This section shows the comparative analysis of proposed work with the existing works in terms of performance metrics like Accuracy, Precision, Recall, AUC, F1-Score respectively.

4.3.1. Performance evaluation in ECG

From the table 2, it is evident that the highest F-score observed for Log energy entropy is 0.032, while the lowest F-score recorded for Kurtosis is 1.50 1008. As a result, Log energy entropy is ranked first, whereas Kurtosis is ranked last.

Tab. 2. Represents the F-Score features and its ranking

S. No	Features	Ranking	F-score
1	Signal energy	7	1.54×10^{-02}
2	Log energy entropy	1	0.036
3	RMS value	5	7.83×10^{-04}
4	Variance	6	1.77×10^{-03}
5	Threshold entropy	4	2.13×10^{-01}
6	Maximum value	8	1.77×10^{-08}
7	Kurtosis	10	1.44×10^{-09}
8	Shannon entropy	9	6.03×10^{-06}
9	Skewness	3	6.17×10^{-4}
10	Sure entropy	2	1.03×10^{-02}

The overall performance analysis of our proposed framework DM detection with the state-of-the-art works such as DL based CNN (Ahamed et al., 2023), DL-Net (Cordeiro et al., 2021), FE-net (Jain et al., 2023), DBSCAN-CNN (Li et al., 2021), Fragment-net (Navaneethakrishna & Manuskandan, 2021) are shown in the table below. The authors assess the evaluation on various performance metrics, including Precision (or specificity), Recall (or sensitivity), Area Under the Curve (AUC), and F-1 score.

From the table 3, it shows clearly that our model's performance in the ECG data has increased Accuracy and it is achieved by employing EX-kNN. EX-kNN will improve the transparency and interpretability through the decision-making process which has clear classification explanations.

Tab. 3. Illustrates the performance metrics of the existing framework and our framework

Model	Acc	Precision	Recall	AUC	F1-Score
DL based CNN (Ahamed et al., 2023)	96.32	94.36	93.25	0.91	92.63
DL-Net (Cordeiro et al., 2021)	95.26	93.65	94.36	0.92	93.54
FE-Net (Jain et al., 2023)	94.36	96.77	95.35	0.94	97.36
DBSCAN-CNN (Li et al., 2021)	98.11	93.25	96.34	0.93	96.38
Fragment-net (Navaneethakrishna & Manuskandan, 2021)	97.25	96.87	94.25	0.92	94.68
Our Method	98.99	97.86	96.97	0.95	98.80

Illustrating the AUC with the best ECG data performance for the various model has been shown in Table 4.For evaluating AUC, it is a commonest method to evaluate the performance of the classification models. It is challenging to provide a specific and most precise value; we indicated a strong performance which has a high AUC value closer to 1.

Tab. 4. Shows the AUC with the best ECG performance

MODEL	AUC
SVM Gaussian	53.26%
SVM polynomial	57.36%
Logistic Regression	63.69%
SVM linear	59.88%
DNN 10layer	94.54%
Our Method	95.66%

The features are arranged in a feature matrix according to their rankings from 1 to 5. Table 5. describes the performance of the ECG parameter ranked from 1 to 5 with the different ML Classifier. This feature matrix is then utilized as input for the machine learning classifier, employing various kernel functions such as Medium Tree (MeT), Coarse Tree (CoT), Linear Discriminant (LiD), Quadratic Discriminant (QuD). The authors assess the robustness of their system by evaluating various performance metrics, including Accuracy, Precision (or specificity), Recall (or sensitivity), Negative Predicted Rate (NPV), Positive Predicted Value (PPV) and F-1 score.

Tab. 5. Demonstrates the performance of the ECG parameter ranked from 1 to 5 in ML classifier

Rank	Classifier	ACC	SEN	SPE	NPV	PPV	F1-Score
1	MeT	64.22	63.88	72.04	18.74	96.74	0.78
	CoT	63.11	65.55	77.99	17.34	97.60	0.75
	LiD	61.77	61.98	59.02	13.13	95.88	0.78
	QuD	61.88	61.94	61.55	10.33	94.58	0.78
2	MeT	63.55	64.33	55.99	30.69	81.44	0.71
	CoT	60.20	61.88	82.14	6.22	98.11	0.74
	LiD	61.44	61.88	56.84	12.54	93.44	0.71
	QuD	61.85	61.11	58.65	12.15	93.33	0.72
3	MeT	77.60	78.32	79.12	60.23	89.36	0.79
	CoT	70.32	92.22	55.32	91.91	55.36	0.77
	LiD	66.36	73.00	74.56	16.39	95.36	0.72
	QuD	66.32	62.35	55.21	31.25	86.25	0.71
4	MeT	79.36	79.44	72.36	61.35	90.58	0.82
	CoT	70.22	91.65	56.54	91.36	55.68	0.79
	LiD	66.32	62.14	74.36	17.35	94.36	0.68
	QuD	68.24	73.26	56.36	59.20	73.69	0.74
5	MeT	88.36	89.44	85.36	82.99	99.10	0.95
	CoT	70.65	91.05	58.36	91.91	55.36	0.71
	LiD	67.39	66.31	82.36	18.36	96.35	0.48
	QuD	65.35	72.65	67.98	52.55	82.39	0.77

By comparing the performance metrics of the proposed work with those of existing works (Ahamed et al., 2023; Cordeiro et al., 2021; Jain et al., 2023; Li et al., 2021; Navaneethakrishna & Manuskandan, 2021), it becomes evident that understanding the improvements, strengths, and weaknesses is depicted. Figure 7 shows the Graphical presentation of the performance Metrics compared with the existing works. The other ECG detecting DM work lacks in removing the remaining refined artifacts, thus resulting in

decreased performance in accuracy and other metrics. In our work, we remove the artifacts after the encoding process, enabling us to achieve better performance.

4.3.2. Performance evaluation in PPG

The comprehensive evaluation of our proposed framework for detecting DM is analyzed with state-of-the-art approaches, including DL-based methods DEL-NET (Srinivasan & Foroozan, 2021), Light CNN (Zanelli et al., 2023), NI-Classifying-Net (Susana et al., 2023), ED-Net (Susana et al., 2022), DW-Net (Khan et al., 2023) are shown in the table 6.

Tab. 6. Represents the performance metrics of the proposed framework with existing methods

Model	Accuracy	Precision	Recall	AUC	F1-Score
DEL-NET (Srinivasan & Foroozan, 2021)	95.36	94.36	94.78	0.93	92.99
Light CNN (Zanelli et al., 2023)	96.35	95.22	93.65	0.97	91.35
NI-Classifying-Net (Susana et al., 2023)	94.77	95.99	94.58	0.96	90.21
ED-Net (Susana et al., 2022)	96.66	96.35	95.55	0.91	92.44
DW-Net (Khan et al., 2023)	97.55	96.44	96.01	0.92	94.21
Proposed method	98.94	97.36	96.32	0.97	95.36

By conducting a graphical representation, the compared proposed method performance metrics is compared with (Khan et al., 2023; Srinivasan & Foroozan, 2021; Susana et al., 2022, 2023; Zanelli et al., 2023). Figure 6 shows the Graphical presentation of the performance Metrics compared with the existing works. The PPG signals in our process shows an immense performance because of the innovative approach in encoder decoder module, whereas the other method doesn't use residual neural network in the architecture.

The comparison of the performance in testing the PPG signal can involve in combining it by traditional methods.to monitor the Scalability of the classifier we analyze the training time. To analyses the model's effectiveness and identifying weakness the observation of the classifier is done. Table 7: determines the comparison of the PPG signal performance among the traditional classifiers.

4.3.3. Performance evaluation in PPG and ECG

The performance evaluation in PPG and ECG is assessed in table 8 with the existing papers (Li et al., 2024; Pal & Mahadevappa, 2023). It is necessary to evaluate the reliability and the accuracy of these physiological monitoring methods. For classifying DM ML algorithm is commonly used. Here we use EX-ML to determine the importance of the feature in the classification decision by assessing their relevance to the nearest feature. By improving the interpretability our model has a high transparency in classification. Whereas, other method uses CNN the classification and detection accuracy is not acquired properly.

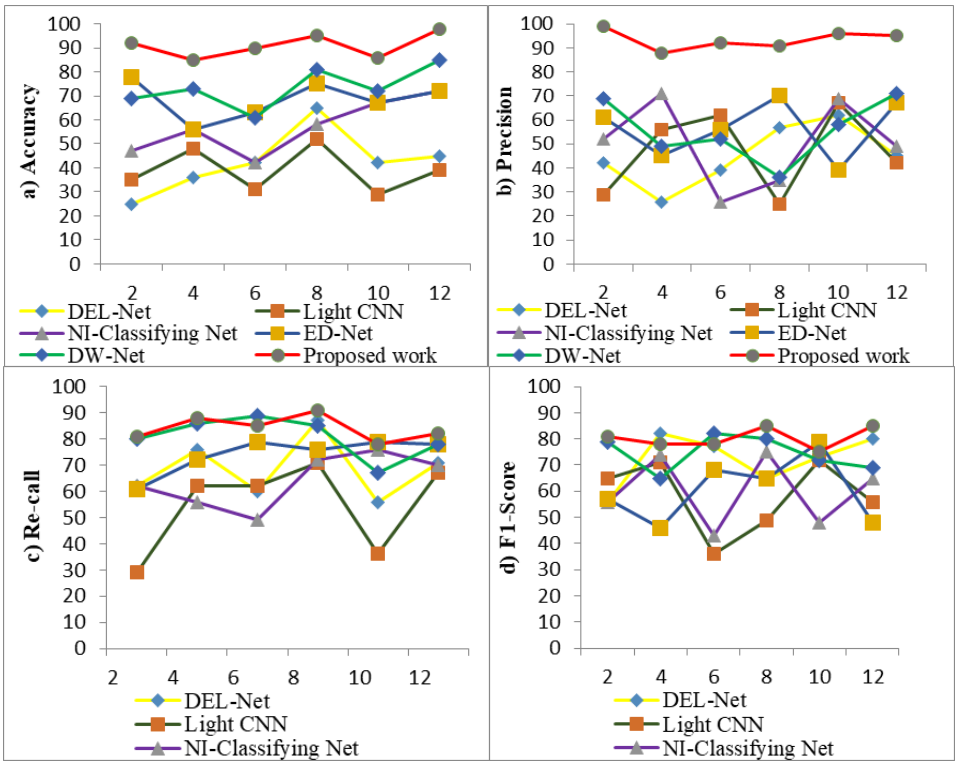

Fig. 7. a) Shows the Graphical presentation of the performance Metrices compared with the existing works Accuracy; b) Denotes the Precision comparison; c) Comparison of Recall; d) F1 score comparison

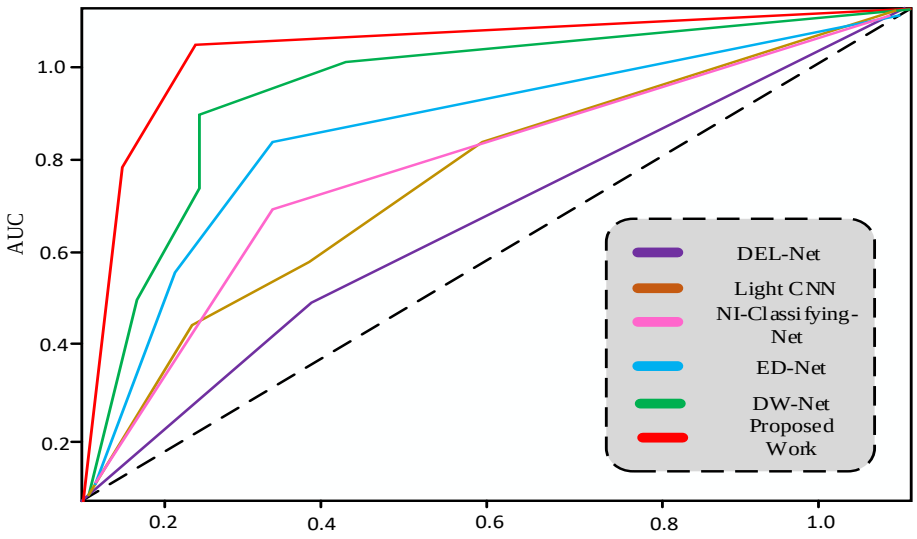

Fig. 8. AUC curve assessment

Tab. 7. Shows the comparison of the PPG signal performance among the traditional classifiers

Classifier	Accuracy	Observations	Training Time	Total Cost
Ensemble Subspace KNN	96.00	~99	8.33	7
Ensemble Bagged Trees	95.00	~270	8.65	9
Fine KNN	98.00	~200	14.00	7
Medium Trees	98.00	~310	25.00	2
Narrow Neural Network	97.00	~330	26.00	NA
Weighted KNN	93.00	~260	16.18	5
3-Layered Neural Network	97.00	~240	2.00	NA
Fine Trees	98.00	~170	7.36	8
Ensemble Boosted Trees	92.00	~360	5.19	2
Coarse Gaussian SVM	90.00	~290	28.36	7
Logistic Regression	91.00	~130	48.36	10
EX-KNN (Our Proposed Method)	98.94	~110	6.35	NA

Tab. 8. Represents the comparison of proposed method performance metrics with the existing methods

Model	Accuracy	Precision	Recall	AUC	F1-Score
Choquet-NET (Li et al., 2024)	94.38	96.36	93.66	0.94	91.87
Dual-DNN (Zanelli et al., 2023)	95.45	96.22	94.75	0.96	94.37
Proposed method	96.84	96.89	95.32	0.97	95.21

4.3.4. Performance on large datasets

The authors analysed their model performance with larger datasets, specifically the Heart Rate Variability (HRV) PPG Dataset (HRV PPG) and the PhysioNet Cardiovascular Signal Challenge Datasets. The HRV PPG dataset provides a substantial amount of data that encompasses various physiological states, including healthy individuals and those with metabolic conditions such as diabetes. When the model is trained on this dataset, we observe significant improvements in key performance metrics, including accuracy, precision, and recall shown in table 9. This dataset allows the model to learn a wider range of physiological variations, which is essential for enhancing its generalizability. Initial evaluations indicate that the model can more effectively differentiate between normal and diabetic states when utilizing the diverse data present in the HRV PPG dataset. The PhysioNet datasets include a rich variety of cardiovascular signals, offering a comprehensive platform for training machine learning models. By leveraging this larger and more diverse dataset, our model demonstrates improved robustness in its predictive capabilities. Through rigorous validation techniques, such as k-fold cross-validation, we have confirmed that the model performs consistently well across different folds, suggesting a lower likelihood of overfitting. Additionally, training on these datasets enables the model to generalize better to unseen data, thereby increasing confidence in its applicability to real-world scenarios.

Tab. 9.Analysis on the HRV PPG dataset and physio net dataset

Model	Accuracy	Precision	Recall	AUC	F1-Score
HRV PPG dataset	96.38	96.26	94.46	0.96	94.81
Physionet Dataset	97.25	96.84	95.75	0.97	95.37

5. CONCLUSION

The combination of PPG and ECG has a unique ability for classifying the DM and this approach has a loaded information embedded in physiological signals and offers a non-invasive and potentially cost effective for assessing the metabolic health. Furthermore, the PPG and ECG-based detection offers several advantages, including probability, ease of use and real-time monitoring capability. However, despite the promising potential of these technologies, several challenges remain, including standardization of data acquisition methods, validation in various populations, etc. The simultaneous analysis of these signals offers valuable insights into the cardiovascular health and the DM-related abnormalities such as autonomic dysfunction and vascular changes. EX-ML algorithm used in this research provides a transparency and interpretability by explaining the reason behind the classification decision. The authors improved the interpretability and allowed the clinicians to understand the features and biomarkers driven for the classification result. From the comparative results it is clear that the advanced method in ML can easily classify and it can achieve high accuracy and the AUC shows the best performance. Finally, the integration of EX-ML technique with the PPG and ECG signals was holding an immense action in improving the classification accuracy and provide a actionable insights. Data variability, model complexity and generalizability are the challenges across various areas of active research and development. Addressing these challenges will be crucial for the widespread adoption of EX-ML approaches in DM classification using PPG and ECG signals.

Conflict of interest

On behalf of all authors, the corresponding author states that there is no conflict of interest.

REFERENCES

Ahamed, A. K. A., Lalitha, K., Saravanan, S., & Muthu Kumar, S. (2023). Enhanced Deep Learning based non-invasive anomaly detection of ECG signals with emphasis on diabetes. *International Journal of Intelligent Systems and Applications in Engineering*, *11*(6s), 284-294.

Cordeiro, R., Karimian, N., & Park, Y. (2021). Hyperglycemia identification using ECG in Deep Learning era. *Sensors*, *21*(18), 6263. https://doi.org/10.3390/s21186263

Dave, D., Vyas, K., Branan, K., McKay, S., DeSalvo, D. J., Gutierrez-Osuna, R., Cote, G. L., & Erraguntla, M. (2024). Detection of hypoglycemia and hyperglycemia using noninvasive wearable sensors: Electrocardiograms and accelerometry. *Journal of Diabetes Science and Technology*, *18*(2), 351–362. https://doi.org/10.1177/19322968221116393

Gupta, S., Singh, A., Sharma, A., & Tripathy, R. K. (2022). dSVRI: A PPG-based novel feature for early diagnosis of type-II diabetes mellitus. *IEEE Sensors Letters*, *6*(9), 1-4. https://doi.org/10.1109/LSENS.2022.3203609

Hina, A., & Saadeh, W. (2022). A 186μW photoplethysmography-based noninvasive glucose sensing SoC. *IEEE Sensors Journal*, *22*(14), 14185-14195. https://doi.org/10.1109/JSEN.2022.3180893

Jain, A., Verma, A., & Verma, A. K. (2023). Non-invasive and automatic identification of diabetes using ECG signals. *International Journal of Electrical and Electronics Research*, *11*(2), 418-425. https://doi.org/10.37391/ijeer.110223

Khan, M., Kumar Singh, B., & Nirala, N. (2023). Expert diagnostic system for detection of hypertension and diabetes mellitus using discrete wavelet decomposition of photoplethysmogram signal and machine learning technique. *Medicine in Novel Technology and Devices*, *19*, 100251. https://doi.org/10.1016/j.medntd.2023.100251

Kulkarni, A. R., Patel, A. A., Pipal, K. V., Jaiswal, S. G., Jaisinghani, M. T., Thulkar, V., Gajbhiye, L., Gondane, P., Patel, A. B., Mamtani, M., & Kulkarni, H. (2023). Machine-Learning algorithm to non-invasively detect diabetes and pre-diabetes from electrocardiogram. *BMJ Innovations*, *9*(1), 32-42. https://doi.org/10.1136/bmjinnov-2021-000759

Lee, P.-L., Wang, K.-W., & Hsiao, C.-Y. (2023). A noninvasive blood glucose estimation system using dual-channel PPGs and pulse-arrival velocity. *IEEE Sensors Journal*, *23*(19), 23570-23582. https://doi.org/10.1109/JSEN.2023.3306343

Li, J., Ma, J., Omisore, O. M., Liu, Y., Tang, H., Ao, P., Yan, Y., Wang, L., & Nie, Z. (2024). Noninvasive blood glucose monitoring using spatiotemporal ECG and PPG feature fusion and weight-based choquet Integral multimodel approach. *IEEE Transactions on Neural Networks and Learning Systems*, *35*(10), 14491-14505. https://doi.org/10.1109/TNNLS.2023.3279383

Li, J., Tobore, I., Liu, Y., Kandwal, A., Wang, L., & Nie, Z. (2021). Non-invasive monitoring of three glucose ranges based on ECG by using DBSCAN-CNN. *IEEE Journal of Biomedical and Health Informatics*, *25*(9), 3340-3350. https://doi.org/10.1109/JBHI.2021.3072628

Mishra, B., & Nirala, N. (2023). Type2 diabetes classification from short photoplethysmogram signal using multiple domain features and Machine Learning techniques. *Research on Biomedical Engineering*, *39*(3), 541-560. https://doi.org/10.1007/s42600-023-00287-7

Mishra, B., Nirala, N., & Singh, B. K. (2024). Type-2 diabetes identification from toe-photoplethysmography using Fourier decomposition method. *Neural Computing and Applications*, *36*(5), 2429-2443. https://doi.org/10.1007/s00521-023-09208-2

Navaneethakrishna, M., & Manuskandan, S. R. (2021). Analysis of heart rate variability in normal and diabetic ECG signals using fragmentation approach. *2021 43rd Annual International Conference of the IEEE Engineering in Medicine & Biology Society (EMBC)* (pp. 1112-1115). IEEE. https://doi.org/10.1109/EMBC46164.2021.9631076

Pal, P., & Mahadevappa, M. (2023). Adaptive multidimensional dual attentive DCNN for detecting cardiac morbidities using fused ECG-PPG signals. *IEEE Transactions on Artificial Intelligence*, *4*(5), 1225-1235. https://doi.org/10.1109/TAI.2022.3184656

Prabha, A., Yadav, J., Rani, A., & Singh, V. (2021). Design of intelligent diabetes mellitus detection system using hybrid feature selection based XGBoost classifier. *Computers in Biology and Medicine*, *136*, 104664. https://doi.org/10.1016/j.compbiomed.2021.104664

Prabha, A., Yadav, J., Rani, A., & Singh, V. (2022). Intelligent estimation of blood glucose level using wristband PPG signal and physiological parameters. *Biomedical Signal Processing and Control*, *78*, 103876. https://doi.org/10.1016/j.bspc.2022.103876

Sathish, D., Poojary, S. S., Shetty, S., Acharya, P. H., & Kabekody, S. (2024). Non-invasive diabetes detection system using photoplethysmogram signals. In S. Tiwari, M. C. Trivedi, M. L. Kolhe, & B. K. Singh (Eds.), *Advances in Data and Information Sciences* (Vol. 796, pp. 457–467). Springer Nature Singapore. https://doi.org/10.1007/978-981-99-6906-7_39

Sen Gupta, S., Kwon, T.-H., Hossain, S., & Kim, K.-D. (2021). Towards non-invasive blood glucose measurement using machine learning: An all-purpose PPG system design. *Biomedical Signal Processing and Control*, *68*, 102706. https://doi.org/10.1016/j.bspc.2021.102706

Shaan, B., Prabha, A., & Yadav, J. (2023). Pulse decomposition analysis based non-invasive diabetes detection system. In S. M. Thampi, J. Mukhopadhyay, M. Paprzycki, & K.-C. Li (Eds.), *International Symposium on Intelligent Informatics* (Vol. 333, pp. 291-302). Springer Nature Singapore. https://doi.org/10.1007/978-981-19-8094-7_22

Shaan, B., Yadav, J., & Prabha, A. (2022). ML based non-invasive diabetes detection system using pulse decomposition analysis of PPG signal. *2022 8th International Conference on Signal Processing and Communication (ICSC)* (pp. 417-422). IEEE. https://doi.org/10.1109/ICSC56524.2022.10009195

Shashikant, R., Chaskar, U., Phadke, L., & Patil, C. (2021). Gaussian process-based kernel as a diagnostic model for prediction of type 2 diabetes mellitus risk using non-linear heart rate variability features. *Biomedical Engineering Letters*, *11*(3), 273-286. https://doi.org/10.1007/s13534-021-00196-7

Singha, S. K., & Ahmad, M. (2021). Noninvasive heart rate and blood glucose level estimation using photoplethysmography. *2021 International Conference on Information and Communication Technology for Sustainable Development (ICICT4SD)* (pp. 151-155). IEEE. https://doi.org/10.1109/ICICT4SD50815.2021.9396849

Srinivasan, V. B., & Foroozan, F. (2021). Deep Learning based non-invasive diabetes predictor using Photoplethysmography signals. *2021 29th European Signal Processing Conference (EUSIPCO)* (pp. 1256-1260). IEEE. https://doi.org/10.23919/EUSIPCO54536.2021.9616351

Susana, E., Ramli, K., Murfi, H., & Apriantoro, N. H. (2022). Non-invasive classification of blood glucose level for early detection diabetes based on photoplethysmography signal. *Information*, *13*(2), 59. https://doi.org/10.3390/info13020059

Susana, E., Ramli, K., Purnamasari, P. D., & Apriantoro, N. H. (2023). Non-invasive classification of blood glucose level based on photoplethysmography using time-frequency analysis. *Information*, *14*(3), 145. https://doi.org/10.3390/info14030145

Zanelli, S., Yacoubi, M. A. E., Hallab, M., & Ammi, M. (2023). Type 2 diabetes detection with light CNN from single raw PPG wave. *IEEE Access*, *11*, 57652-57665. https://doi.org/10.1109/ACCESS.2023.3274484